Pyruvate Site of Pyruvate Phosphate Dikinase: Crystal Structure of the Enzyme−Phosphonopyruvate Complex, and Mutant Analysis[†,‡]

Osnat Herzberg,*[,§] Celia C. H. Chen,[§] Sijiu Liu,[§] Aleksandra Tempczyk,[§] Andrew Howard,[||] Min Wei,[⊥] Dongmei Ye,[⊥] and Debra Dunaway-Mariano[⊥]

Center for Advanced Research in Biotechnology, University of Maryland Biotechnology Institute, 9600 Gudelsky Drive, Rockville, Maryland 20850, Department of Chemistry, University of New Mexico, Albuquerque, New Mexico 87131, Illinois Institute of Technology, Chicago, Illinois 60616, and Advanced Photon Source, Argonne National Laboratory, 9700 South Cass Avenue, Argonne, Illinois 60439

Received September 17, 2001; Revised Manuscript Received November 5, 2001

ABSTRACT: Crystals of pyruvate phosphate dikinase in complex with a substrate analogue inhibitor, phosphonopyruvate ($K_i = 3\ \mu M$), have been obtained in the presence of Mg^{2+}. The structure has been determined and refined at 2.2 Å resolution, revealing that the Mg^{2+}-bound phosphonopyruvate binds in the α/β-barrel's central channel, at the C-termini of the β-strands. The mode of binding resembles closely the previously proposed PEP substrate binding mode, inferred by the homology of the structure (but not sequence homology) to pyruvate kinase. Kinetic analysis of site-directed mutants, probing residues involved in inhibitor binding, showed that all mutations resulted in inactivation, confirming the key role that these residues play in catalysis. Comparison between the structure of the PPDK−phosphonopyruvate complex and the structures of two complexes of pyruvate kinase, one with Mg^{2+}-bound phospholactate and the other with Mg^{2+}-oxalate and ATP, revealed that the two enzymes share some key features that facilitate common modes of substrate binding. There are also important structural differences; most notably, the machinery for acid/base catalysis is different.

PPDK[1] catalyzes the interconversion of ATP, P_i, and pyruvate, with AMP, PP_i, and PEP, in three Mg^{2+}-dependent partial reactions that involve phospho- and pyrophospho-enzyme intermediates (*1*, *2*):

$$\text{E−His} + \text{ATP} \rightarrow \text{E−His−PP·AMP} \quad \text{(I)}$$

$$\text{E−His−PP·AMP} + P_i \rightarrow \text{E−His−P·AMP·PP}_i \quad \text{(II)}$$

$$\text{E−His−P} + \text{pyruvate} \rightarrow \text{E−His} + \text{PEP} \quad \text{(III)}$$

The above reactions are reversible, and the outcome depends on the host organism (glycolytic ATP synthesis, or PEP synthesis). Enzyme phosphorylation and pyrophosphorylation occur on a histidine residue, His455 (*3*). The nucleotide binding site is located within the N-terminal part of the polypeptide chain, whereas the pyruvate/PEP binding site is located within the C-terminal part of the chain (*4*−*7*).

The crystal structure of PPDK in the unbound state (*8*) revealed two remote substrate binding sites, one binding site for ATP/AMP and P_i/PPi and the second for pyruvate/PEP. The two binding sites are located 45 Å apart, and each is associated with a different structural domain. The N-terminal segment of the polypeptide chain contains a 240-residue nucleotide binding domain that adopts the fold termed ATP-grasp (*9*). The C-terminal 340-residue pyruvate/PEP binding domain adopts an α/β-barrel fold. A third domain contains the phosphoryl/pyrophosphate group acceptor/donor residue, His455. The locations of the nucleotide binding sites were inferred by analogy to other enzymes with the folds of the ATP-grasp, and the location of the PEP/pyruvate binding site by analogy to α/β-barrel enzymes. The structure implies that the phosphohistidine domain undergoes a swivel motion to shuttle the phosphoryl group between the two remote active sites.

The pyruvate/PEP binding site of PPDK may be compared with the active site of pyruvate kinase, an enzyme that converts PEP to ATP directly, without the involvement of a phosphoenzyme intermediate. The pyruvate kinase active site also adopts an α/β-barrel fold (*10*). The comparison revealed conservation of several key residues involved in substrate binding, and similarity in their relative disposition in the active site. Thus, a model has been developed for the pyruvate/PEP binding to PPDK based on the information from pyruvate kinase site (*8*). Binding studies in the

[†] Supported by NSF Grant MCB9813271 (O.H.) and NIH Grant GM36260 (D.D.-M.). Use of the National Synchrotron Light Source was supported by the U.S. Department of Energy, Basic Energy Sciences, Office of Science, under Prime Contract DE-AC02-98CH110886, by the National Science Foundation, and by National Institutes of Health Grant 1P41 RR12408-01A1. Use of the Advanced Photon Source was supported by the U.S. Department of Energy, Basic Energy Sciences, Office of Science, under Contract W-31-109-Eng-38.

[‡] The coordinates have been deposited in the Protein Data Bank (entries 1KBL and 1KC7).

* To whom correspondence should be addressed. Telephone: (301) 738-6245. Fax: (301) 738-6255. E-mail: osnat@carb.nist.gov.

[§] University of Maryland Biotechnology Institute.

[||] Illinois Institute of Technology and Argonne National Laboratory.

[⊥] University of New Mexico.

[1] Abbreviations: PPDK, pyruvate phosphate dikinase; PEP, phosphoenolpyruvate; ATP, adenosine 5′-triphosphate; AMP, adenosine 5′-monophosphate; P_i, inorganic phosphate; PP_i, inorganic pyrophosphate; Hepes, *N*-(2-hydroxyethyl)piperazine-*N*′-ethanesulfonic acid.

10.1021/bi011799+ CCC: $22.00
Published on Web 12/19/2001

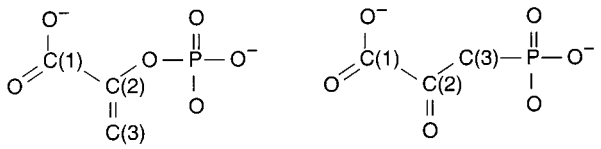

FIGURE 1: Structures of PEP and P-pyr, the substrate and inhibitor of PPDK, respectively.

crystalline state proved to be illusive, probably due to the relatively high K_m value of the substrate (~30 μM), and the fact that, so far, crystals useful for X-ray work have been obtained only from solutions containing a high concentration of ammonium sulfate (~2 M). The high ionic strength of the crystallization solution is expected to lead to reduced substrate affinity, as the substrate and Mg^{2+} cofactor are charged.

The current work became possible following the discovery that phosphonopyruvate (P-pyr), a compound that resembles PEP (Figure 1), inhibits PPDK activity at micromolar concentrations (K_i = 3 μM). The crystal structure of the PPDK−P-pyr complex, together with site-directed mutagenesis data, confirms the location of the pyruvate/PEP binding sites, and the identity of the residues that play key roles in catalysis. Also reported is the structure of the apoenzyme at 1.94 Å resolution. This is a better resolution than that of our previously reported structure (*8*), thus facilitating a more reliable comparison between the bound and unbound enzyme.

MATERIALS AND METHODS

Expression, Protein Purification, and Site-Directed Mutagenesis. Wild-type and mutant PPDK proteins from *Clostridium symbiosum* were expressed in *Escherichia coli* and purified as described previously (*11*). Mutant proteins were prepared from the plasmid pACYC184-D12 using a PCR-based procedure analogous to that described in ref *5*. Primers for mutagenesis, 18−22 base pairs in length, were synthesized by Gibco BRL Life Science. *Kpn*I and *Bst*XI restriction sites were employed in the construction of the E745Q, D769A, N768A, D620N, R617K, R561K, and C831A mutants. The sequences of the isolated mutant genes were determined by the Center for Agricultural Biotechnology at the University of Maryland (College Park, MD). The mutant genes were expressed in *E. coli* JM101 cells as described in ref *5*. Proteins were purified to homogeneity as judged by SDS−PAGE analysis. The observed chromatographic properties of the mutant proteins were indistinguishable from those of wild-type PPDK.

Crystallization and X-ray Data Collection. Crystallization of the wild-type protein in the unbound state was as reported previously (*8*). The enzyme−inhibitor crystals were obtained similarly, but in the presence of Mg^{2+} and phosphonopyruvate. Single crystals were obtained at 30 °C by vapor diffusion in sitting drops. The protein drops were equilibrated against a reservoir solution containing 54% saturated ammonium sulfate and a 100 mM Hepes buffer (pH 7.0). The drop consisted of protein at a concentration of 9 mg/mL, 20 mM imidazole buffer (pH 6.5), 100 mM KCl, 40 mM phosphonopyruvate, 5 mM $MgCl_2$, 0.1 mM EDTA, and 1 mM DTT, diluted with an equal volume of reservoir solution. For data collection, crystals of apo-PPDK and of the enzyme−inhibitor complex were transferred to a cryogenic solution comprising 60% saturated ammonium sulfate, 20% glycerol, and 0.1 M Hepes buffer (pH 7.0). In addition, the cryogenic solution for the enzyme−inhibitor complex also contained 40 mM P-pyr and 40 mM $MgCl_2$. After soaking in the cryogenic solution for 2 h, the crystal was flash-cooled in liquid propane cooled by liquid nitrogen. As with the crystal of the apoprotein, the space group of the enzyme−inhibitor crystal was *P*2, with one monomer in the asymmetric unit. The unit cell dimensions of the unbound protein crystal were as follows: a = 89.8 Å, b = 58.7 Å, c = 102.9 Å, and β = 94.8°. For the enzyme−inhibitor complex crystal, the cell dimensions were as follows: a = 89.2 Å, b = 58.4 Å, c = 102.6 Å, and β = 95.0°.

X-ray intensity data for both apoenzyme and enzyme−inhibitor crystals were collected at 100 K. The native data were collected to 1.9 Å resolution on the X12C beamline of the National Synchrotron Light Source (NSLS, Brookhaven National Laboratory, Upton, NY), and the enzyme−inhibitor complex data were collected to 1.73 Å resolution on the IMCA-CAT 17-ID beamline at the Advanced Photon Source (Argonne National Laboratory). Diffraction data at a wavelength of 1.3 Å at NSLS beamline X12C were recorded on a 300 mm MAR research image plate, and at the IMCA-CAT 17-ID beamline, diffraction data at a wavelength of 1.0 Å were recorded on a MAR 165 mm charge-coupled device system. For the PPDK−inhibitor complex, several crystals were tested, and they all exhibited high mosaic spread. For the best diffracting crystal, the estimated mosaic spread was close to 2.5°. This was the crystal used for data acquisition. Data collected on the X12C beamline were processed with HKL (*12*). Data collected on the IMCA-CAT beamline were processed with the X-GEN package (*13*). The statistics of data processing are given in Table 1. R_{merge} values for the PPDK−inhibitor data indicate poor quality beyond ~1.9 Å resolution, which is attributed to the high mosaic spread of the crystal. Although refinement commenced using all data up to 1.8 Å resolution, it was ultimately completed at a truncated resolution of 2.2 Å.

Structure Determination and Refinement. The starting model for refinement was that of the room-temperature wild-type apo-PPDK structure refined at 2.3 Å resolution (PDB entry 1DIK), excluding solvent molecules. The structures were refined with the program CNS (*14*). Two cycles of simulated annealing at 2500 K were followed by positional and individual temperature factor refinement cycles. For the refinement of the PPDK−P-pyr complex, high *R*-factor values were apparent when data were being refined at 1.8 Å resolution (for example, the simulated annealing cycles resulted in an R_{free} of 0.350 and a conventional R of 0.319). Nevertheless, the quality of the electron density map was very good, revealing clear density for four residues (506−509) that were disordered in the original model derived from data collected at room temperature. In addition, main chain modifications were required in three other positions. Because of the high mosaic spread of the crystal, and the associated high *R*-factor values at the higher-resolution shells, the data resolution was gradually reduced to 2.2 Å.

The progress of the refinement was evaluated by the improvement in the quality of the electron density maps and the reduced values of the conventional *R*-factor ($R = \sum_h||F_o| - |F_c||/\sum_h|F_o|$, where F_o and F_c are the observed and

Table 1: Data Processing Statistics

Apo-PPDK (processed with HKL)

temperature (K)	100
wavelength (Å)	1.3
cell dimensions	$a = 89.8$ Å, $b = 58.7$ Å, $c = 102.9$ Å, $\beta = 94.8°$

shell lower limit (Å)	no. of unique reflections	completeness (%)	$\langle I/\sigma(I)\rangle$	R_{merge}[a]
4.09	8373	96.1	35.8	0.028
3.25	8245	96.7	37.2	0.034
2.84	8238	96.8	28.2	0.050
2.58	8144	96.3	19.4	0.075
2.39	8098	95.7	13.9	0.098
2.25	7968	94.5	10.4	0.128
2.14	7863	93.3	7.6	0.174
2.05	7830	92.8	5.7	0.240
1.97	7767	92.1	3.9	0.340
1.90	6736	80.1	2.9	0.405
total	79262	93.5	23.7	0.051

PPDK−P-pyr (processed with X-GEN)

temperature (K)	100
wavelength (Å)	1.0
cell dimensions	$a = 89.2$ Å, $b = 58.4$ Å, $c = 102.5$ Å, $\beta = 95.0°$

shell lower limit (Å)	no. of unique reflections	completeness (%)	$\langle I/\sigma(I)\rangle$	R_{merge}[a]
3.15	18 226	98.0	73.7	0.057
2.50	18 064	98.5	34.9	0.115
2.18	17 893	98.0	21.2	0.184
1.98	17 776	97.5	13.3	0.271
1.84	17 668	97.1	7.3	0.412
1.73	14 814	81.4	4.1	0.523
total	104 444	95.1	26.6	0.114

[a] $R_{merge} = \sum_h\sum_i|\langle I(h)\rangle - I(h)_i|/\sum_h\sum_i I(h)_i$ for equivalent observations.

calculated structure factor amplitudes, respectively) and R_{free} (*15*). The electron density maps were inspected and the models modified on an interactive graphics workstation with the program O (*16*) for the apoenzyme structure and the program TURBO-FRODO (*17*) for the enzyme−inhibitor complex. Two types of electron density maps with $2|F_o| - |F_c|$ and $|F_o| - |F_c|$ coefficients and with calculated phases were inspected simultaneously. Density for Mg^{2+} and the P-pyr was apparent from the initial map of the complex structure. These were added to the model at the third positional refinement cycle. Sulfate ions and water molecules were added gradually as the refinement progressed. They were assigned in the $|F_o| - |F_c|$ difference Fourier maps with a 3σ cutoff level for inclusion in the model.

Steady-State Kinetic Measurements. Initial velocities were measured for the AMP + PP_i + PEP → ATP + P_i + pyruvate reaction as a function of the concentration of the varied substrate (in a range of 0.5−10 times K_m) at fixed, saturating concentrations of the cosubstrates (0.5 mM AMP, 0.5 mM PEP, and 1 mM PP_i) and metal ion cofactors (5 mM $MgCl_2$ and 40 mM NH_4Cl) in 20 mM imidazole (pH 6.8, 25 °C). The initial velocity data were analyzed using eq 1 and the computer programs of Cleland (*18*). The k_{cat} was calculated from V_{max}/[E].

$$v_o = (V_{max}[E][S])/(K_m + [S]) \quad (1)$$

where v_o is the initial velocity, [E] is the enzyme concentration, [S] is the substrate concentration, V_{max} is the maximum velocity, and K_m is the Michaelis constant.

The K_i value for the competitive inhibitor P-pyr (*19*) was determined from initial velocity data obtained at varying PEP concentrations, and fixed, saturating concentrations of cosubstrates and cofactors. The initial velocity data were analyzed using eq 2 where K_i is the inhibition constant and [I] the inhibitor concentration.

$$v_o = (V_{max}[E][S])/[K_m(1 + [I]/K_i) + [S]] \quad (2)$$

Single-Turnover Reactions of [^{14}C]PEP. [^{14}C]PEP was synthesized from [^{14}C]pyruvate (obtained from NEN Life Science Products) as described in ref *2*. The single-turnover reactions of 40 μM wild-type PPDK, 5 μM [^{14}C]PEP, 5 mM $MgCl_2$, and 40 mM NH_4Cl in 50 mM K^+Hepes (pH 7.0, 25 °C) were carried out in a rapid quench instrument from KinTek Instruments. Mixtures for reactions carried out with the mutant enzymes were mixed by hand and the reactions quenched by hand. Reactions were initiated by mixing 32 μL of buffered enzyme/cofactors with 32 μL of buffered substrate and then terminated at specific reaction times with 182 μL of 0.6 M HCl. The protein was removed from the reaction mixture by centrifugal size filtration using a 500 μL filter (molecular mass cutoff of 30 kDa) purchased from Pall Gelman Inc. [^{14}C]PEP and [^{14}C]pyruvate were separated from the filtrate on a Beckman Ultrasil anion-exchange HPLC column using 0.3 M KH_2PO_4 and 0.6 M KCl (pH 5.0) as the mobile phase. [^{14}C]PEP- and [^{14}C]pyruvate-containing fractions were assayed for radioactivity by liquid scintillation counting. The concentration of [^{14}C]pyruvate formed in each reaction was calculated by multiplying the initial substrate concentration by the percent conversion. Time course data were fitted to a single-exponential equation (eq 3) using KaleidaGraph to yield the rate constants (k_{obs}) for the single-turnover reaction.

$$[B]_t = [B]_\infty[1 - \exp(-k_{obs}t)] \quad (3)$$

where $[B]_t$ and $[B]_\infty$ correspond to the pyruvate concentration at time t and at equilibrium, respectively.

Single-Turnover Reactions of [^{14}C]ATP in the Presence of P_i. [^{14}C]ATP (specific activity of 500 μCi/mmol) was synthesized from [^{14}C]AMP (obtained from NEN Life Science Products) as described in ref *2*. Single-turnover reactions of 40 μM wild-type or mutant PPDK, 10 μM [^{14}C]-ATP, 11 mM P_i, 5 mM $MgCl_2$, and 40 mM NH_4Cl were carried out using the KinTek rapid quench device as described in the previous section. The protein was removed from the reaction mixture by centrifugal size filtration. The unconsumed [^{14}C]ATP and product [^{14}C]AMP were separated by HPLC using a Beckman ultrasphere C18 reversed-phase column and 25 mM KH_2PO_4, 2.5% triethylamine, and 5% methanol (pH 4.1) as the mobile phase. The fractions containing ATP and AMP were quantitated for ^{14}C radioactivity by liquid scintillation counting. The k_{obs} value for the single-turnover reaction was computed as described in the previous section.

RESULTS AND DISCUSSION

Quality of the Model. The final structure of the apoenzyme includes all but the N- and C-terminal residues of the 874-

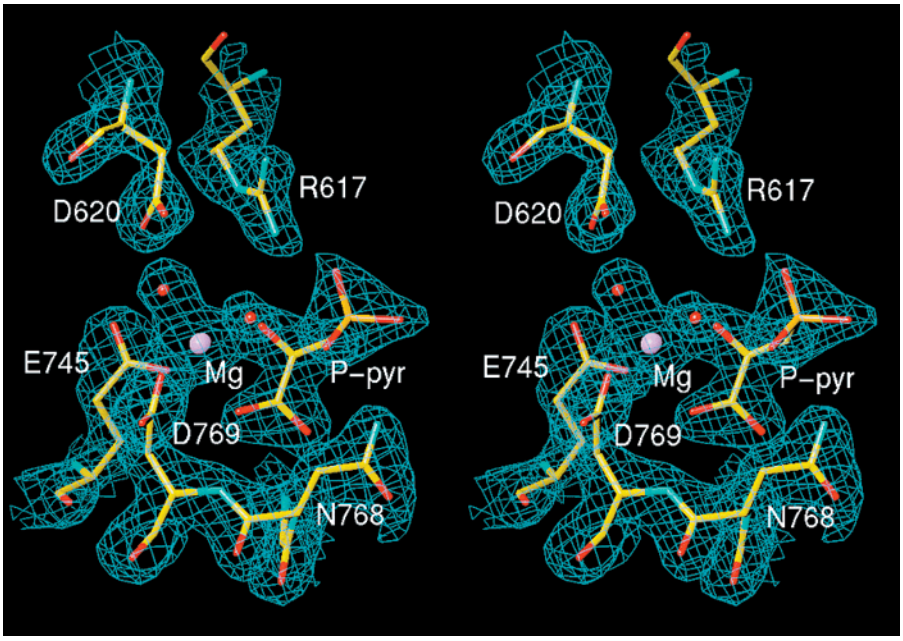

FIGURE 2: Electron density map associated with the inhibitor and its environment, together with the final model. The $2F_o - F_c$ coefficients and calculated phases are used. The map is contoured at the 1σ level.

amino acid protein, five sulfate ions, one ammonium ion, and 879 water molecules. The conventional *R*-factor is 0.194, for the 67 245 reflections at 1.94 Å resolution for which $F \geq 2\sigma(F)$ (84.4% completion), and R_{free} for 5139 reflections (6.5% of the reflections) is 0.257. The stereochemical parameters are well within the range known from crystal structures of small peptides. The root-mean-square deviation (rmsd) values in bond length and bond angle are 0.223 Å and 2.0°, respectively. The model of the enzyme−inhibitor complex includes all but the N- and C-terminal residues, the Mg^{2+}-bound phosphonopyruvate, five sulfate ions, and 645 water molecules. Electron density associated with some or all of the side chains of some surface residues was absent; thus, the occupancies of the corresponding atoms were set to 0. The conventional *R*-factor is 0.198, for the 49 319 reflections at 2.2 Å resolution for which $F \geq 2\sigma(F)$ (91.5% completion), and R_{free} for 2584 reflections (4.8% of the reflections) is 0.269. The rmsds values in bond length and bond angle are 0.018 Å and 1.9°, respectively. The electron density map in the region of the bound inhibitor is shown in Figure 2.

The rmsd in bond length between the apoprotein and bound protein structures is 0.3 Å for α-carbon atoms, and 0.5 Å for all atoms. Thus, the overall structure is the same within the accuracy of the data resolution. There are only subtle changes in the conformation of binding site residues that can be attributed to Mg^{2+}−P-pyr binding.

Mode of Inhibitor Binding. As is seen typically with α/β-barrels, the inhibitor binds in a crevice at the center of the barrel, close to the carboxyl termini of the β-strands (Figure 3a). The Mg^{2+} and the pyruvate moiety bind deep in the crevice, while the phosphonate group is exposed to solvent. As the inhibitor is a close analogue of the PEP, we propose that for the true substrate, the phosphoryl group also projects toward the barrel opening and is available for transfer from and to the histidine domain of PPDK when it aligns to interact with the pyruvate/PEP domain.

A rich network of interactions ensures the precise positioning of the P-pyr. Mg^{2+} mediates inhibitor binding by forming octahedral coordination (average Mg−ligand distance of 2.3 Å) to protein carboxyl groups (Glu745 and Asp769), to two oxygen atoms of the pyruvate moiety of P-pyr [bidentate coordination to C(1)O and to C(2)O], and to two water molecules (Figure 3b). The water molecules are further bridged, one interacting with the phosphonyl group of P-pyr and the other with Glu745 and Asp620. For PEP, the true substrate, the phosphoryl group would be covalently attached to the oxygen atom of C(2), and would coordinate directly to Mg^{2+}. This coordination is consistent with conclusions derived from electron paramagnetic resonance spectroscopy measurements of the phosphorylated enzyme complex with oxalate (*20*).

Note that in the apo-PPDK structure, a solvent molecule interacts with three protein carboxylate groups (Asp620, Glu745, and Asp769), a sulfate ion, and two solvent molecules. The crystallographic temperature factor and interaction distances of this solvent molecule (but not the geometry) are consistent with ammonium ion. Superposition with the protein−inhibitor complex structure shows that the postulated ammonium ion is located 2.1 Å from the position of the Mg^{2+} in the complex structure, and the sulfate ion is located 2.2 Å from the phosphonyl group. Thus, the environment of the ammonium and sulfate ions resembles but is not identical to that of the Mg^{2+} and P-pyr phosphonyl group shown in Figure 3b. The side chains of Glu745 and Asp769 adjust slightly to form the interactions with the ammonium ion, whereas the conformation of Asp620 remains the same.

Enzyme activity is enhanced in the presence of ammonium (*21*). Moskovitz and Wood proposed that the cation is required for enolization of pyruvate, but the position of the observed ammonium ion in apo-PPDK is inconsistent with such a role. The ammonium ion seen in the apo-PPDK must be displaced upon magnesium binding, as indeed is observed in the enzyme−inhibitor crystal structure. The role of the

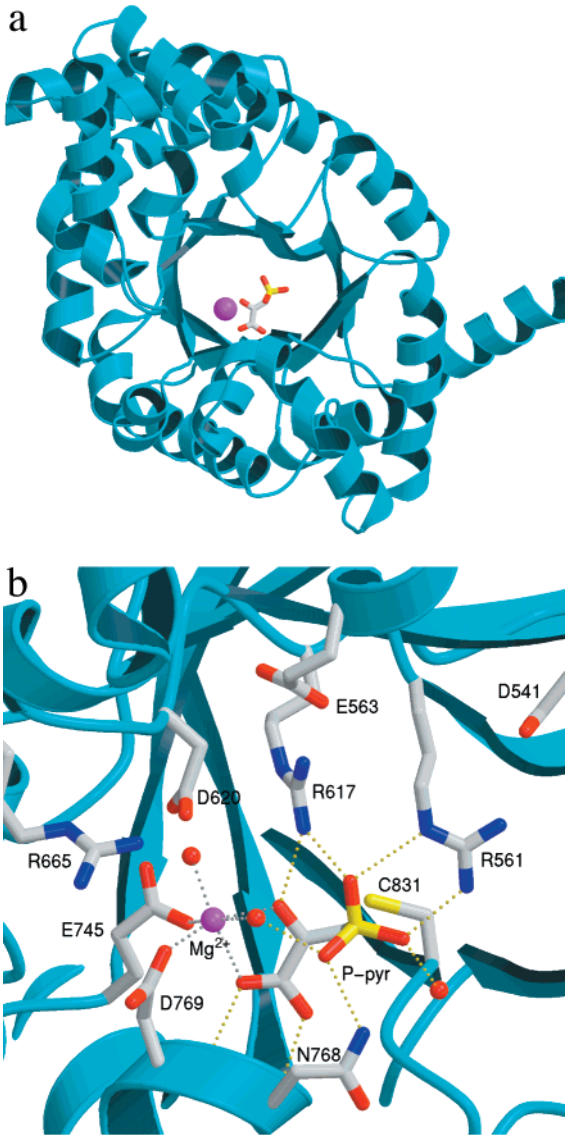

FIGURE 3: Binding mode of P-pyr. (a) Location of the inhibitor in the context of the overall fold of the pyruvate/PEP domain. P-pyr is shown as a stick model. Atomic colors are as follows: oxygen, red; carbon, white; sulfur, yellow; and Mg^{2+}, magenta. (b) Atomic detail of the environment of Mg^{2+}-bound P-pyr. Atomic colors are as described for panel a. Coordinations to the cation are shown as gray dotted lines, and electrostatic interactions with P-pyr are shown as yellow dotted lines.

ammonium ion in the activation of PPDK remains unclear. Binding of the monovalent cation should interfere with magnesium binding. On the other hand, for structural integrity, binding of a cation may always be necessary because the environment in the center of the α/β-barrel is crowded, and includes several negatively charged residues. In the intact barrel, Glu745, Asp769, and Asp620 are located close to one another, a potentially unstable arrangement unless a counter charge is present.

In addition to the interaction with Mg^{2+}, the pyruvate moiety forms two other important interactions. (i) The carboxylate group is positioned at the N-terminus of a short α-helix following the sixth β-strand of the barrel (not part of the α/β-barrel secondary motifs) such that it forms electrostatic interactions with the two helical main chain nitrogen atoms (Asn768 and Asp769). (ii) The C(2) carbonyl oxygen atom interacts with the guanidinium group of Arg617.

The three oxygen atoms of the phosphonyl group form multiple interactions with the side chains of Arg617, Arg561, and Asn768 and with three water molecules (for clarity, one water molecule is not shown in Figure 3b). Slight adjustment of the side chains or the substrate may accompany binding of PEP, because of the different dispositions a phosphoryl group and the phosphonyl group.

A second interaction shell supports the conformational integrity of side chains involved directly in Mg^{2+} and P-pyr binding. Particularly striking is the extensive charge network that governs the binding site. All of the residues that form this charge network are invariant in the PPDKs that have been sequenced to date, and most of them are also conserved in the closely related enzyme phosphoenolpyruvate synthase.

The side chain of the invariant Cys831 is located deeper in the active site, just below the P-pyr, and close to C(3) (4 Å). Because of its location relative to a modeled substrate, we proposed earlier a catalytic role for the thiol group in providing a proton to the enolate form of pyruvate (*8*). Cys831 is surrounded by three hydrophobic residues: Leu559, Met704, and Met743 (omitted from Figure 3 for clarity). The Cys831 sulfur atom also interacts with the hydroxyl group of Ser764 (3.5 Å), an invariant residue in all PPDK sequences (Figure 4). Ser764 is buried and interacts with a buried water molecule (2.5 Å), which in turn interacts with the main chain oxygen atom of Gly558 (2.6 Å, not shown in the figure) and with the hydroxyl group of Tyr851 (3.0 Å). Tyr851 is exposed to solvent and is hydrogen bonded to a surface water molecule. We propose that the acid/base catalysis by Cys831 may be mediated by dissipating a proton through this intricate hydrogen bond network.

Kinetic Properties of Active Site Mutants. C-Terminal domain active site residues Arg561 (*7*), Arg617, Asp620, Glu745, Asn768, Asp769, and Cys831 (*8*), which interact with the substrate, coordinate to Mg^{2+}, or support a coordinating water molecule (Asp620), were replaced by site-directed mutagenesis with alanine, or with residues of like charge, or isosteric side chain, to generate R561K, R617K, N768A, C831A, D620A, E745Q, and D769A. The characterization of mutants that probe an enzyme with two remote active sites, such as PPDK, requires that in addition to measurement of the global effect of the mutation, the reaction rates at each of the two different active sites be measured as well. The expectation is that a mutation that alters the pyruvate/PEP catalytic machinery would not affect the nucleotide active site.

The purified mutant enzymes were evaluated for catalysis of the AMP + PP_i + PEP → ATP + P_i + pyruvate reaction using steady-state kinetic techniques. The k_{cat} measured by this method is determined by the rate at which catalysis occurs at the N-terminal domain nucleotide active site (partial reactions I and II), as well as by the rate at which catalysis occurs at the C-terminal domain pyruvate/PEP active site (partial reaction III). Previous studies (*22*) have shown that for wild-type PPDK, these two rates are comparable, and thus, a mutation that impairs catalysis at the C-terminal domain active site will reduce the k_{cat} measured for the complete reaction.

Table 2 shows that amino acid replacement at Arg561, Arg617, Glu745, Asn768, and Cys831 severely inhibits

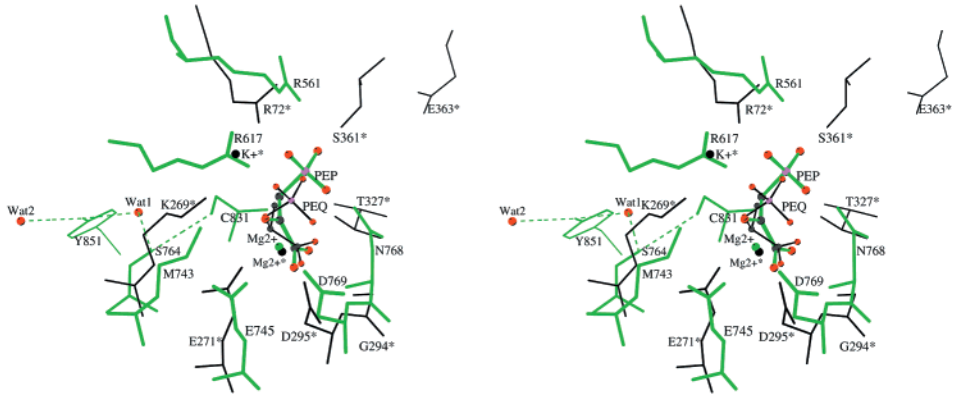

FIGURE 4: Stereoscopic representation of the superposition of the active sites of PPDK−P-pyr and pyruvate kinase−phospholactate structures. PPDK residues are colored green, and pyruvate kinase residues are colored black. Oxygen atoms of P-pyr and phospholactate are colored red, and the phosphorus is colored magenta. The hydrogen bond network from Cys831 to the solvent accessible water molecule is shown as green dash lines. Phospholactate is labeled PEQ, and pyruvate kinase residues are labeled with asterisks.

Table 2: Kinetics of Wild-Type and Mutant PPDKs in Catalysis of the AMP + PP_i + PEP → ATP + P_i + Pyruvate Reaction

enzyme	k_{cat} (s^{-1})	$^{PEP}K_m$ (μM)	$^{P-pyr}K_i$ (μM)
wild-type[a]	25 ± 1	27.0 ± 0.5	5 ± 0.6
D620N[b]	0.24 ± 0.06	110 ± 10	14 ± 2
D769A[c]	0.045 ± 0.003	570 ± 20	
R561K[d]	<0.02		
R617K[d]	<0.02		
E745Q[d]	<0.02		
N768A[d]	<0.02		
C831A[d]	<0.02		

[a] The reaction mixtures initially contained 0.5 mM AMP, 1.0 mM PP_i, 10−100 μM PEP, 40 mM NH_4Cl, 5 mM $MgCl_2$, and 20 mM imidazole-HCl (pH 6.8, 25 °C). [b] The reaction mixtures initially contained 0.5 mM AMP, 1.0 mM PP_i, 50−500 μM PEP, 40 mM NH_4Cl, 5 mM $MgCl_2$, and 20 mM imidazole-HCl (pH 6.8, 25 °C). [c] The reaction mixtures initially contained 0.5 mM AMP, 1.0 mM PP_i, 0.2−2.5 mM PEP, 40 mM NH_4Cl, 5 mM $MgCl_2$, and 20 mM imidazole-HCl (pH 6.8, 25 °C). [d] The reaction mixtures initially contained 0.5 mM AMP, 1.0 mM PP_i, 1 mM PEP, 40 mM NH_4Cl, 5 mM $MgCl_2$, and 20 mM imidazole-HCl (pH 6.8, 25 °C).

catalysis of the full reaction. Indeed, only the D620A and D769A PPDK mutants are sufficiently active for k_{cat} (decreased 100- and 500-fold, respectively) and $^{PEP}K_m$ (increased 4- and 21-fold, respectively) determination. And, only the activity of D620A PPDK enabled P-pyr K_i determination (increased 3-fold).

Catalysis at the C-terminal domain active site and catalysis at the N-terminal domain active site of each mutant PPDK were separately evaluated by measuring the rates and equilibrium positions for the partial reactions

$$E + [^{14}C]PEP \rightarrow E-P + [^{14}C]pyruvate$$

and

$$E + [^{14}C]ATP + P_i \rightarrow E-P + [^{14}C]AMP + PP_i$$

The apparent rate constants (k_{obs}) and equilibrium constants (K_{eq}) measured for these reactions are reported in Tables 3 and 4.

The k_{obs} and K_{eq} values measured for catalysis at the nucleotide active site (Table 4) are essentially the same in the wild-type enzyme and the mutants, indicating that the mutations made at the C-terminal domain have no significant effect on the functioning of the N-terminal and central domains.

Table 3: Rate Constants for Wild-Type, and Mutant PPDKs in Catalysis of the E + [^{14}C]PEP → E−P·[^{14}C]Pyruvate Reaction[a]

enzyme	k_{obs} (s^{-1})	K_{eq}	enzyme	k_{obs} (s^{-1})	K_{eq}
wild-type	43	0.35	R617K	4.5×10^{-3}	0.56
E745Q	6.1×10^{-4}	0.26	N768A	3.2×10^{-3}	0.46
D769A	6.3×10^{-4}	0.30	R561K[b]	NA	
D620N	1.0×10^{-3}	0.46	C831A[b]	NA	

[a] The reaction mixtures initially contained 40 μM enzyme, 5 μM [^{14}C]PEP, 5 mM $MgCl_2$, and 40 mM NH_4Cl in 50 mM K^+Hepes (pH 7.0, 25 °C). [b] Not active.

Table 4: Single-Turnover Rate Constants for Wild-Type and Mutant PPDKs in Catalysis of the E + [^{14}C]ATP + P_i → E−P + [^{14}C]AMP + PP_i Reaction[a]

enzyme	k_{obs} (s^{-1})	enzyme	k_{obs} (s^{-1})
wild-type	6.0	R617K	8.4
E745Q	7.6	N768A	8.4
D769A	4.3	R561K	5.4
D620N	7.3	C831A	3.2

[a] The reaction mixtures initially contained 20 μM enzyme, 5 μM [^{14}C]ATP, 11 mM P_i, 5 mM Mg^{2+}, 40 mM NH_4^+, and 50 mM K^+HEPES (pH 7.0, 25 °C). All reactions generated ca. 3.2 μM AMP as product.

The k_{obs} and K_{eq} values measured for catalysis at the pyruvate/PEP active site are dramatically reduced compared with those measured for the wild-type enzyme (Table 3). The enzyme contributes to the reaction equilibrium E + [^{14}C]PEP ⇆ E·[^{14}C]PEP ⇆ E−P·[^{14}C]pyruvate ⇆ E−P + [^{14}C]pyruvate as a substrate and a product. Thus, the overall K_{eq} is determined by the dissociation constants of E·[^{14}C]PEP (170 μM) and E−P·[^{14}C]pyruvate (75 μM), and by the internal equilibrium constant which equals [E−P·[^{14}C]pyruvate]/[E·[^{14}C]PEP] which equals 1 (*11*). A change in K_{eq} indicates that a change in one or more of these thermodynamic constants has occurred. Under the reaction conditions that were employed, the K_{eq} for the partial reaction (i.e., total amount of [^{14}C]pyruvate/total amount of [^{14}C]PEP) catalyzed by wild-type PPDK is 0.35 and the k_{obs} for the conversion of [^{14}C]PEP to [^{14}C]pyruvate is 43 s^{-1}. The equilibrium constant value is decreased 14% for E769A PPDK and 26% for E745Q PPDK. The values for D620A and N768A PPDK are both increased by 31%, while that for R617K PPDK is increased by 60%.

Substrate binding is not rate-limiting for the PEP partial reaction (*22*). The rate at which equilibrium is reached (k_{obs}) is thus determined by the effectiveness of the catalytic groups, and the Mg^{2+} and NH_4^+ cofactors, in activating the substrate and stabilizing the transition state. The mechanism of phosphoryl transfer from PEP to the PPDK His455 has not yet been investigated. In addition to the C-terminal domain's amino acid residues, residues on the central domain are also likely to be involved. For the present discussion, a minimal mechanism, in which proton transfer [to PEP C(3)] and phosphoryl transfer [from the PEP C(2) oxygen atom] occur in the same transition state, will be assumed. The k_{obs} values measured for the active site mutants are all much smaller than that of wild-type PPDK, indicating that consistent with the structural information, each of the replaced residues plays an essential role in catalysis.

Relationship to Pyruvate Kinase. Pyruvate kinase is a key metabolic enzyme that converts PEP to ATP, as does PPDK. Although the overall reaction catalyzed by these two enzymes is similar, pyruvate kinase differs from PPDK in that it acts by transferring the phosphoryl group directly from PEP to ADP to produce ATP without the involvement of phospho- and pyrophospho-enzyme intermediates. Also, pyruvate kinase catalyzes a reaction that is essentially irreversible; on the other hand, the equilibrium constant for the PPDK reaction enables the reaction to be driven in both directions, and the outcome depends on the needs of the host organism. *C. symbiosum*, the source of the enzyme studied here, lacks pyruvate kinase, and PPDK functions in glycolytic ATP synthesis.

The pyruvate/PEP binding domains of both pyruvate kinase and PPDK form α/β-barrels. Of the 340 amino acid of the PPDK PEP binding domain, 192 can be superposed on pyruvate kinase with an rmsd of 2.1 Å for the paired α-carbon atoms. The sequences of the superposed residues are only 15% identical. Despite the lack of significant overall amino acid sequence identity, some of the key active site amino acid residues are identical and the mode of Mg−pyruvate binding is essentially the same (Figure 4). The comparison of the PPDK−P-pyr complex with the structure of pyruvate kinase bound to a compound similar to PEP, phospholactate (*10*), shows that the two Mg^{2+}-coordinating carboxylate-containing residues are conserved in the two enzymes. Glu745 and Asp769 of PPDK have their pyruvate kinase equivalents in Glu271 and Asp295, respectively. Moreover, the N-terminus of a short helix provides an oxyanion hole that anchors the carboxylate group of the pyruvate moiety of the substrate in both cases (the main chain nitrogen atoms of Asn768 and Asp769 in PPDK and those of Gly294 and Asp295 in pyruvate kinase).

The superposition of the two enzymes shows that the guanidinium groups of Arg617 and Arg561 are located in positions equivalent to those of K^+ and Arg72 in pyruvate kinase, respectively. The PPDK site-directed mutants altered at positions 617 and 561 yielded proteins with very low activity (Tables 2 and 3), even though the replacements retained positively charged side chains (lysine). Previously, we proposed, on the basis of PEP modeled in the active site, that Arg617 and Arg561 provide favorable charge interactions with the phosphoryl group to be transferred (*8*). This is now substantiated by the crystallographic and kinetic results, as well as by the analogy to pyruvate kinase.

Interestingly, the enzymatic activities of both enzymes are stimulated by specific monovalent cations (*21*, *23*). As Arg617 of PPDK replaces K^+ in pyruvate kinase, the role of the monovalent ion in PPDK ought to be different than in pyruvate kinase. This issue needs to be investigated further.

Finally, the identity of the residues responsible for general acid/base catalysis is more apparent in PPDK than in pyruvate kinase. In pyruvate kinase, Lys269 may be excluded from such a role because it lies on the 2-*re* face of the prospective enolate (*10*, *24*). Indeed, the equivalent position in PPDK is occupied by a methionine residue, Met743, not a likely catalytic residue (Figure 4). The current proposal for pyruvate kinase acid/base machinery was developed on the basis of the structure of the enzyme in complex with Mg^{2+}, ATP, and oxalate (*24*). The authors propose that Thr327 and Ser361 may participate in proton relay to the remotely located, invariant Glu363, with the involvement of two bridging water molecules. The superposition of the two enzyme structures shows Thr327 of pyruvate kinase to be ~6 Å away from Cys831, and Ser361 is located even farther away. The pyruvate kinase residue that overlaps with Cys831 of PPDK is a methionine (Met290), again not a residue that is likely to be catalytic. Thus, acid/base catalysis in PPDK and pyruvate kinase appears to be provided by different residues.

ACKNOWLEDGMENT

We thank the staff at the National Synchrotron Light Source, beamline X12C, and the staff at the Advanced Photon Source, IMCA-CAT, for their help during data collection.

REFERENCES

1. Wood, H. G., O'Brien, W. E., and Michaeles, G. (1977) *Adv. Enzymol. 45*, 85−155.
2. Carroll, L. J., Mehl, A. P., and Dunaway-Marioano, D. (1989) *J. Am. Chem. Soc. 111*, 5965−5967.
3. Carroll, L. J., Xu, Y., Thrall, S. H., Martin, B. M., and Dunaway-Mariano, D. (1994) *Biochemistry 33*, 1134−1142.
4. McGuire, M., Carroll, L. J., Yankie, L., Thrall, S. H., Dunaway-Mariano, D., Herzberg, O., Jayaram, B., and Haley, B. H. (1996) *Biochemistry 35*, 8544−8552.
5. McGuire, M., Huang, K., Kapadia, G., Herzberg, O., and Dunaway-Mariano, D. (1998) *Biochemistry 37*, 13463−13474.
6. Xu, Y., Yankie, L., Shen, L., Jung, Y. S., Mariano, P. S., Dunaway-Mariano, D., and Martin, B. M. (1995) *Biochemistry 34*, 2181−2187.
7. Yankie, L., Xu, Y., and Dunaway-Mariano, D. (1995) *Biochemistry 34*, 2188−2194.
8. Herzberg, O., Chen, C. C., Kapadia, G., McGuire, M., Carroll, L. J., Noh, S. J., and Dunaway-Mariano, D. (1996) *Proc. Natl. Acad. Sci. U.S.A. 93*, 2652−2657.
9. Murzin, A. G. (1996) *Curr. Opin. Struct. Biol. 6*, 386−394.
10. Larsen, T. M., Laughlin, L. T., Holden, H. M., Rayment, I., and Reed, G. H. (1994) *Biochemistry 33*, 6301−6309.
11. Pocalyko, D. J., Carroll, L. J., Martin, B. M., Babbitt, P. C., and Dunaway-Mariano, D. (1990) *Biochemistry 29*, 10757−10765.
12. Otwinowski, Z., and Minor, W. (1997) *Methods Enzymol. 276*, 307−326.
13. Howard, A. J. (1996) in *Proceedings from the Macromolecular Crystallographic Computing School* (Watenpaugh, P. E. B. a. K. D., Ed.) Oxford University Press, New York (in press).

14. Brünger, A. T., Adams, P. D., Clore, G. M., DeLano, W. L., Gros, P., Grosse-Kunstleve, R. W., Jiang, J. S., Kuszewski, J., Nilges, M., Pannu, N. S., Read, R. J., Rice, L. M., Simonson, T., and Warren, G. L. (1998) *Acta Crystallogr. D54*, 905−921.
15. Brünger, A. T. (1992) *Nature 355*, 472−474.
16. Jones, T. A., Zou, J. Y., Cowan, S. W., and Kjeldgaard, M. (1991) *Acta Crystallogr. A47*, 110−119.
17. Roussel, A., and Cambillau, C. (1989) *TURBO-FRODO*, Silicon Graphics, Mountain View, CA.
18. Cleland, W. W. (1979) *Methods Enzymol. 63*, 103−138.
19. Sparkes, M. J., Rogers, K. L., and Dixon, H. B. (1990) *Eur. J. Biochem. 194*, 373−376.
20. Kofron, J. L., Ash, D. E., and Reed, G. H. (1988) *Biochemistry 27*, 4781−4787.
21. Moskovitz, B., and Wood, H. (1978) *J. Biol. Chem. 253*, 884−888.
22. Mehl, A., Xu, Y., and Dunaway-Mariano, D. (1994) *Biochemistry 33*, 1093−1102.
23. Boyer, P. d., Lardy, H. A., and Phillips, P. H. (1942) *J. Biol. Chem. 146*, 673−682.
24. Larsen, T. M., Benning, M. M., Rayment, I., and Reed, G. H. (1998) *Biochemistry 37*, 6247−6255.

BI011799+